Applied Catalysis B: Environmental 91 (2009) 47–58

Contents lists available at ScienceDirect

Applied Catalysis B: Environmental

journal homepage: www.elsevier.com/locate/apcatb

Detailed surface reaction mechanism for Pt-catalyzed abatement of automotive exhaust gases

J. Koop, O. Deutschmann *

Institute for Chemical Technology and Polymer Chemistry, University of Karlsruhe, Karlsruhe Institute of Technology (KIT), Germany

ARTICLE INFO

Article history:
Received 9 December 2008
Received in revised form 28 April 2009
Accepted 1 May 2009
Available online 9 May 2009

Keywords:
Modeling
Platinum
Catalysis
Reaction mechanism
Automotive pollutants
Nitrogen oxides
DETCHEM

ABSTRACT

A modeling and simulation study on Pt-catalyzed conversion of automotive exhaust gases is presented. The model is based on a newly developed surface reaction mechanism consisting of 73 elementary-step like reactions among 22 surface and 11 gas-phase species. Reactions for the conversion of the major pollutants CO, CH_4, C_3H_6, and NO_x are included. The mechanism is implemented in a two-dimensional flow field description of a single channel of the catalytic monolith. The model is evaluated by comparison with data derived from isothermal laboratory experiments in a flat bed reactor with platinum-coated monoliths using synthetic lean/rich cycling exhaust gas mixtures. The influence of CO and C_3H_6 at lean and H_2 at rich conditions on NO conversion is investigated, both at steady-state conditions. Furthermore, the model is also applied for the simulation of emissions of hydrocarbons, CO, and NO from a gasoline engine (stoichiometric exhaust gas) in a dynamic engine test bench.

1. Introduction

Mostly driven by environmental concerns, the demand for noble metal catalysts has been increased continuously in the last decades. A typical catalyst for passenger cars contains about 2 g of noble metal [1]. Today, platinum is used as precious metal component in three-way catalysts (TWC), diesel oxidation catalysts (DOC), NO_x storage catalysts (NSC), and also as catalyst for coated particulate filters (cDPF) [2].

Due to the outstanding importance of platinum as oxidation and reduction component in automotive applications, a detailed understanding of the interactions between chemical reactions and mass and heat transport at operating conditions is indispensable. Hence, we present a concept for modeling and numerical simulation of catalytic converters by describing the coupling of the physical and chemical processes in detail. In recent years, many studies have been published on modeling of catalytic converters [3–8]. In most studies global reactions were applied for the description of the chemistry. These models, however, are only valid in the range of conditions used for the fitting of the global rate coefficients and cannot be applied as a predictive simulation tool at different conditions, e.g. temperatures or gas compositions. Therefore, in the present study a reaction mechanism of "quasi-elementary" steps is applied which describes the reactions on a molecular level under the assumption that the state of the surface is locally characterized by mean values (mean-field approximation) [9]. The main advantage of these detailed reaction mechanisms is their potential to predict the behavior of the chemical system for a wide range of external conditions, sometimes not accessible to experiments. The disadvantage of using elementary chemical reactions is the large number of reaction equations and therefore the need of information on a large number of rate coefficients of the elementary-steps. In literature examples of successful application of elementary-step reaction mechanisms can be found, ranging from simple catalytic conversion of H_2 and O_2 [10,11] to complex simulation of solid oxide fuel cells [12].

For the simulation, we apply the code DETCHEM^{CHANNEL} which is part of the DETCHEM software package [13] which is a FORTRAN based package that is designed to couple detailed chemistry models and computational fluid dynamics (CFD). The core is a library for the description of species properties based on atomistic models and for reactions among gas-phase and surface species based on elementary-step reaction mechanisms. Upon this, the two-dimensional flow field in a single channel is modeled using the boundary-layer assumption. Transport models include composition- and temperature-dependent transport coefficients in the gas phase and an effectiveness factor approach for the washcoat.

* Corresponding author at: Institute for Chemical Technology and Polymer Chemistry, University of Karlsruhe, Engesserstr. 20, 76131 Karlsruhe, Germany. Tel.: +49 721 608 3138; fax: +49 721 608 4805.
E-mail address: olaf.deutschmann@kit.edu (O. Deutschmann).
URL: http://deutschmann.itcp.uni-karlsruhe.de

0926-3373/$ – see front matter © 2009 Elsevier B.V. All rights reserved.
doi:10.1016/j.apcatb.2009.05.006

The aim of this work was to develop a detailed surface reaction mechanism for platinum based on elementary-step like reactions. This mechanism is applied for the simulation of isothermal experiments with a Pt/Al_2O_3 model catalyst (identifier: 10319) in a laboratory reactor and a realistic lean and rich exhaust gas. Moreover, to further test the reliability of the kinetic model, data from engine test bench experiments with a commercial platinum catalyst (identifier: HPT) under stoichiometric conditions were used for comparison with the corresponding simulation results.

2. Experimental

The catalyst used in this study is a platinum γ-alumina washcoat carried by a monolithic honeycomb structure (10319). The washcoat is supported on a cordierite monolith with a cell density of 400 cpsi[1] and 6 mil[2] wall thickness. The catalyst has been manufactured with commercial techniques and was provided by Delphi Catalyst. For the production of the model catalyst neither stabilizers nor oxygen storage components were added. The specifications of this catalyst are summarized in Table 1. The Pt/Al_2O_3 model catalyst has been hydrothermally treated at 700 °C for 4 h. A noble metal dispersion of 16% was measured by CO chemisorption assuming an adsorption stoichiometry of one CO molecule per Pt adsorption site [14]. BET surface area of 49 m^2/g and mean BJH pore diameter of 6.4 nm were determined by N_2 physisorption. In addition to this model catalyst, a commercial platinum three-way catalyst without ceria washcoat was used (HPT). This catalyst is loaded with 40 g platinum/ft^3 catalyst. The commercial Pt/Al_2O_3 has been aged for 4 h at 850 °C.

The experimental investigations[3] of the kinetics are carried out under isothermal conditions in a flat bed reactor [15] using a realistic model exhaust gas, given in Table 2. The synthetic gas matrix of a Diesel engine for lean and rich phase includes CO, CO_2, O_2, H_2O, NO, NO_2 and C_3H_6 as the representative for unburnt hydrocarbon species. In the rich phase also hydrogen from the homogeneous water-gas-shift reaction during combustion is included. The measured temperature rise during the rich phase was due to the thermal inertia of the reactor not higher than 10 K. Furthermore, lateral outlets allow the measurement of gas concentration profiles along the length of the catalyst. The experimental system is equipped with a fast responding mass spectrometer for the measurement of short lean/rich cycles. The space velocity is 40,000 h^{-1}.

In the laboratory experiments the model catalyst (10319) has been investigated under cycling conditions with a phase length of 300 s lean and 15 s rich phase. Moreover, measurements under steady-state conditions with a constant lean or rich gas composition (Tables 3 and 4) have been carried out. During the steady-state experiments the mole fractions of CO, C_3H_6 in the lean and H_2 in the rich phase, respectively, were varied in order to investigate the influence of the components on the conversion of nitrogen oxide.

In addition to the experiments in a laboratory-scale apparatus, measurements of the commercial platinum catalyst (HPT) at an engine test bench have been performed. The test bench was equipped with a medium size gasoline engine. Temperatures were measured with fast responding thermocouples placed directly in front of and behind the monolith. The catalyst dimensions are 11.2 cm in diameter and 4.2 cm in length. As test program the NEDC (New European Driving Cycle) consisting of an urban and extra urban driving cycle was chosen [16]. However, in addition to the commercial Pt/Al_2O_3 catalyst an uncoated monolith without any catalytic activity was implemented. The effect of the prior installed monolith on the thermal behavior of the platinum catalyst is a slower temperature increase during the NEDC. Light-off temperatures of the catalytic reactions can be observed in more detail and compared to the temperatures predicted by numerical simulations.

[1] 62 channels/cm^2.
[2] 0.1524 mm.
[3] The experimental investigations of the model catalyst were accomplished at the Institute for Chemical Process Engineering at the University of Stuttgart and published elsewhere [15].

Table 1
Specifications of the Pt/Al_2O_3 model catalyst (10319).

Diameter [a](mm)	1.0
Length (m)	0.2
Noble metal loading (g/ft^3)	80
Platinum dispersion (%)	16
Median pore diameter (nm)	10
Porosity of the washcoat (%)	40

[a] Diameter of the coated channel.

Table 2
Composition of the synthetic exhaust gas; balance: N_2.

Lean/rich cycle	NO (ppm)	NO_2 (ppm)	C_3H_6 (ppm)	CO (%)	CO_2 (%)	H_2 (%)	H_2O (%)	O_2 (%)
Lean	200	40	60	0.04	7	0	10	12
Rich	200	40	60	2.1	7	0.7	10	0.9

Table 3
Composition of the synthetic exhaust gas for the steady-state lean phase; balance: N_2.

Lean	NO (ppm)	NO_2 (ppm)	C_3H_6 (ppm)	CO (%)	CO_2 (%)	H_2 (%)	H_2O (%)	O_2 (%)
C_3H_6-Var.	200	0	0 60 90	0.04	7	0	10	12
CO-Var.	200	0	60	0.00 0.04 0.08	7	0	10	12

3. Mathematical and numerical model

3.1. Flow field model

The reactive flow field in the single catalytic channel with cylindrical symmetry is modeled by the steady-state, two-dimensional boundary-layer equations [13,17–19]. Surface reactions are modeled by an elementary-step reaction mechanism based on the molecular processes using the mean-field approximation implemented in the computer package DETCHEM [13].

In the boundary layer of a fluid near a surface, the convection is mainly directed parallel to the surface. The diffusive transport in this direction is diminished in comparison with the one perpendicular to the surface. This effect becomes more significant as the axial gas velocity is increased, i.e. for higher Reynolds numbers as long as the flow is laminar. The results achieved by the boundary-layer model can be as accurate as the results from the

Table 4
Composition of the synthetic exhaust gas for the steady-state rich phase; balance: N_2.

Rich steady-state	NO (ppm)	NO_2 (ppm)	C_3H_6 (ppm)	CO (%)	CO_2 (%)	H_2 (%)	H_2O (%)	O_2 (%)
H_2-Var.	200	0	60	2.1	7	0 0.7 1.0	10	0.9

full Navier–Stokes model at high but laminar flow rates [17]. These conditions are well-satisfied for all cases studied.

Usually the surface of the solid catalyst is coated with a layer of high surface area material, the washcoat, in which the catalyst is dispersed. The washcoat thickness varies from 10 to 150 μm and can exhibit a non-uniform thickness around the perimeter of the cell. Transport of chemical species inside the washcoat is taken into account by applying an effectiveness factor, η, where the solution of a one-dimensional reaction–diffusion equation for a representative species is expressed in terms of the Thiele modulus [20]. Our model approach leads to the following conservation equation for a single channel simulation:

Continuity equation

$$\frac{\partial(\rho u)}{\partial z} + \frac{1}{r}\frac{\partial(r\rho\upsilon)}{\partial r} = 0, \tag{1}$$

Axial momentum

$$\rho u\frac{\partial u}{\partial z} + \rho\upsilon\frac{\partial u}{\partial r} = -\frac{\partial p}{\partial z} + \frac{1}{r}\frac{\partial}{\partial r}\left(\mu r\frac{\partial u}{\partial r}\right), \tag{2}$$

Radial momentum

$$0 = -\frac{\partial p}{\partial r}, \tag{3}$$

Species continuity

$$\rho u\frac{\partial Y_i}{\partial z} + \rho\upsilon\frac{\partial Y_i}{\partial r} = \frac{1}{r}\frac{\partial(r\, j_{i,r})}{\partial r}, \tag{4}$$

with the diffusion mass flux at the interface of free fluid flow and washcoat being

$$j_{i,r} = \eta\dot{s}_i\tilde{M}_i F_{\mathrm{cat/geo}}. \tag{5}$$

$F_{\mathrm{cat/geo}}$ denotes the ratio between the catalytic surface area of the noble metal and the geometrical area of the cylindrical wall. The transport coefficients (μ and λ) and the radial species diffusion fluxes $j_{i,r}$ depend on temperature and gas-phase composition.

3.2. Surface chemistry model

The chemical source terms due to surface reactions ($\dot{s}_i$) in Eq. 5 and the surface coverages (Θ_i) are modeled by elementary-step based reaction mechanisms.

$$\dot{s}_i = \sum_{k=1}^{K_s}\nu_{i_k}k_{\mathrm{f}_k}\prod_{i=1}^{N_g+N_s}c_i^{\nu'_{i_k}} \tag{6}$$

$$\frac{\mathrm{d}\Theta_i}{\mathrm{d}t} = \frac{\dot{s}_i\sigma_i}{\Gamma} \tag{7}$$

Definition of all variables is given in Table 5.

The state of the catalytic surface is described by its temperature and the coverage of adsorbed species which vary along the channel. The chemical source terms $\dot{s}_i$ of gas-phase species due to adsorption/desorption and surface species are given by Eqs. (6) and (7). The surface reactions on the noble metal are assumed to be in steady-state, thus, the left term of Eq. (7) is zero in this case. The temperature dependence of the rate coefficients is described by a modified Arrhenius expression:

$$k_{\mathrm{f}_k} = A_k\exp\left[-\frac{E_{\mathrm{a}_k}}{RT}\right]\prod_{i=1}^{N_s}\Theta_i^{\mu_{i_k}}\exp\left[\frac{\varepsilon_{i_k}\Theta_i}{RT}\right] \tag{8}$$

This expression takes a potential coverage dependence of the reaction order and the activation energy into account using the parameters μ_{i_k} and ε_{i_k}, respectively.

Table 5
Notation.

A_c	Cross-sectional area (m^2)
A_k	Pre-exponential factor (cm, mole, s)
c_i	Concentration of species i (mole/m^2, mole/m^3)
C_p	Species enthalpy (J/kg K)
E_{a_k}	Activation energy (kJ/mole)
$F_{\mathrm{cat/geo}}$	Ratio of catalytic and geometrical area
h_i	Species enthalpy (J/kg)
$j_{i,r}$	Radial diffusion flux (moles/m^2 s)
k_{f_k}	Forward reaction rate coefficient
k_{r_k}	Reverse reaction rate coefficient
K_s	Number of surface reactions
$\tilde{M}_i$	Species molecular weight (kg/moles)
N_g	Number of gas-phase species
N_s	Number of surface species
p	Pressure (Pa)
r	Channel radius (m)
R	Universal gas constant (J/mol K)
$\dot{s}_i$	Surface reaction rate (moles/m^2 s)
T	Temperature (K)
t	Time (s)
u	Axial velocity (m/s)
Y_i	Mass fraction of species
Y_{is}	Species mass fraction at catalyst surface
z	Axial coordinate (m)
Γ	Surface site density(mole/m^2)
ε_{i_k}	Parameter for coverage-dependent activation energy (kJ/mole)
η	Effectiveness factor
Θ_i	Surface coverage with species i
λ	Thermal conductivity (J/m s K)
μ	Viscosity (kg/m s)
μ_{i_k}	Parameter for coverage-dependent reaction order
ν'_{i_k}	Stoichiometric coefficient for the reactants
ν''_{i_k}	Stoichiometric coefficient for the products
ρ	Density (kg/m^3)
σ_i	Number of occupied surface sites
υ	Radial velocity (m/s)
$\dot{\omega}_i$	Gas-phase reaction rate (moles/m^3 s)
Indices	
i	Species number
k	Reaction number

3.3. Surface reaction mechanism

For the numerical simulation of the oxidation and reduction reactions of exhaust gas species on platinum, a detailed reaction mechanism consisting of 73 elementary-step reactions among 22 surface and 11 gas-phase species has been applied. The elementary-step reaction scheme is based upon a previously published mechanism [21]. In this study an extended gas matrix was used for the simulated exhaust gas, e.g. reactions for the conversion of nitrogen oxide with oxygen and reduction reactions with hydrogen as well as steam reforming reactions were added. Furthermore, the kinetic data of the detailed reaction mechanism have been modified in order to accomplish a thermodynamic consistent data set.

The applied elementary-step mechanism includes dissociative adsorption of CH_4, O_2, H_2 and non-dissociative adsorption of NO, NO_2, N_2O, CO, CO_2, C_3H_6, H_2O and desorption of all species except CH_4. Gas-phase reactions can be neglected due to the low pressure and temperature in automotive catalytic converters. All reactions on platinum are modeled as reversible reactions. The developed mechanism can be subdivided into four parts:

- the decomposition of hydrocarbons via abstraction of hydrogen atoms,
- the oxidation of carbon monoxide to carbon dioxide,
- the formation of water via an adsorbed hydroxyl species (OH),
- reactions for the conversion of nitrogen oxides.

3.3.1. Hydrocarbon decomposition and oxidation

The exhaust gas of a combustion engine contains typically more than 100 different hydrocarbon species depending on many factors [22–24]. In general, as representative hydrocarbon species propylene or a mixture of propylene and methane is often chosen. Representing reactive HCs like olefins or aromatic hydrocarbons, C_3H_6 is used, and methane represents the less reactive hydrocarbons like alkanes. The oxidation of propylene proceeds in analogy to the previously published mechanism of Chatterjee et al. [21] and consists of two reaction pathways. On one hand, adsorption comes along with abstraction of an H-atom and formation of $C_3H_5(s)$. After cracking the C–C bond all remaining carbonatoms are oxidized to CO and CO_2. On the other hand, propylene adsorbs dissociatively on platinum. During the adsorption process a hydrogen atom separates and reacts with an adsorbed oxygen atom to form a hydroxyl species. Since the further progress of this reaction is unknown, the direct oxidation of $C_3H_4(s)$ is modeled as lumped step.

Furthermore, dissociative adsorption of CH_4 was added to the reaction mechanism. Schoofs et al. [25] investigated the adsorption of methane and observed the direct formation of CH_3. The sticking coefficient of this reaction is low compared to other gas-phase species and was taken from Deutschmann et al. [26]. Hickman and Schmidt [27] showed that the adsorption of CH_4 on platinum is an irreversible process. Under investigated reaction conditions it can also be assumed that oxidation reactions are fast and recombination of $CH_3(s)$ and H(s) are unlikely to occur.

3.3.2. Carbon monoxide oxidation

Carbon monoxide is converted via a widely accepted Langmuir–Hinshelwood reaction step [28]. The sticking coefficient on a platinum surface revealed by Campbell et al. [29] is 0.84. In our mechanism we applied a coverage-dependent activation energy of desorption of 136 kJ/mol. The activation energy of the reaction also depends on the coverages with CO and NO.

3.3.3. Reactions including hydroxyl species

Rinnemo et al. studied the dissociative adsorption of hydrogen and oxygen on Pt with sticking coefficients of 0.046 and 0.07 [10]. In the rich phase with high H_2 concentrations, the reaction of adsorbed oxygen (O(s)) with a hydrogen atom (H(s)) plays an important role for the ignition of the hydrogen conversion. An activation energy of 70.5 kJ/mol arose from simulations and is also confirmed by investigations from Salomons et al. [30]. Moreover, water is formed by the reaction of a hydroxyl species with H(s). The activation barrier of 17 kJ/mol is significantly lower compared to the recombination reaction of OH(s) with $E_a = 48$ kJ/mol. In reducing atmosphere and at higher temperatures platinum is able to catalyze the water-gas-shift (WGS) reaction [31]. Zeigarnik et al. [32] formulated an elementary-step reaction scheme for the WGS reaction on platinum and used the semi-empirical method UBI-QEP for the calculation of activation energies which were adopted for our mechanism.

3.3.4. Reactions for the conversion of nitrogen oxides

In the lean phase nitrogen oxide is oxidized to nitrogen dioxide but at temperatures of about 350 °C the conversion is restricted by the thermodynamic equilibrium (cp. Fig. 1). The reaction pathway of the NO oxidation is still under consideration whether it is a Langmuir–Hinshelwood (LH) or Eley–Rideal (ER) reaction type. Most authors assume an ER mechanism in which NO from the gas-phase reacts with an adsorbed oxygen atom [21,33–35]. However, several indications in literature for a LH reaction step can be found as well [36–38]. Especially quantum mechanical calculation based models take reaction of adsorbed NO(s) and O(s) into account [39–42]. In this work, we therefore modeled the NO oxidation by a combined LH and ER reaction scheme. The activation energies of the forward and reverse reactions of NO(s) and O(s) are based on calculations from Mei et al. [40] on Pt(1 1 1) surfaces. The forward reaction is highly activated with 133 kJ/mol and is additionally limited by increasing surface coverage with carbon monoxide. But more crucial, the backward reaction is less activated and constitutes an effective source of surface oxygen on platinum, even in an oxygen-rich atmosphere due to the decomposition of NO_2 [37,43,44]. The main route for the oxidation of nitrogen oxide is the Eley–Rideal pathway indicated by its activation energy of 111 kJ/mol compared to the backward reaction with 115 kJ/mol. But more decisive, the oxidation of NO in the ER reaction mechanism is facilitated by high oxygen surface coverage. Under lean gas composition adsorbed oxygen is the most abundant species which could reduce the activation energy of the oxidation up to 60 kJ/mol (at $\Theta_{O(s)} = 1$).

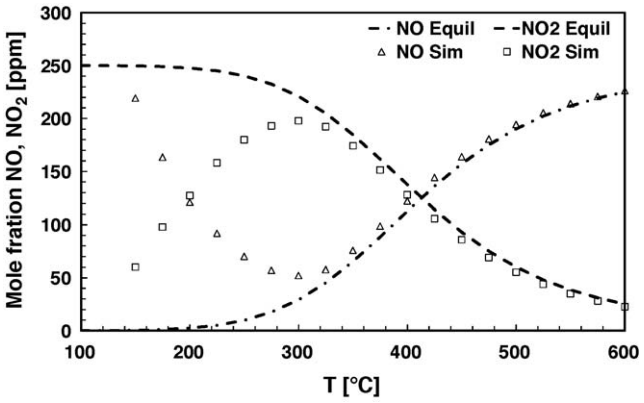

Fig. 1. Comparison of the thermodynamic equilibrium concentrations (—) and simulated concentrations of NO (△) and NO_2 (□) as a function of temperature (250 ppm NO, 12 vol.% O_2 in Argon).

In case of rich gas composition no nitrogen oxidation takes place, because oxygen is primarily reacting with CO and C_3H_6. Thus, NO reacts with the reducing agents hydrogen, propylene and carbon monoxide. However, only the reduction with H_2 is a direct surface reaction, since adsorbed hydrogen lowers the activation barrier for the cleavage of the N–O bond to form N(s) compared to direct NO(s) dissociation [45]. Kinetic data have been taken from bond order conservation Morse potential by Shustorovich and Bell for a Pt(1 1 1) surface [45]. Since CO is blocking adsorption sites for hydrogen [46], the reaction is strongly inhibited by the presence of carbon monoxide. On the other hand, conversion of nitrogen oxides with CO or C_3H_6, like in three-way catalyst or HC-SCR[4] applications, are based upon dissociation of NO_x on a locally oxygen and carbon monoxide free platinum surface [47]. Desorption energy of surface bounded nitrogen atoms depends on the CO surface coverage. This assumption is based upon the consideration that a strongly bounded surface atom like carbon monoxide lowers the Fermi level. By the diminishment of the electron density, the Pt–N bond is weakened which leads to reduced activation energy for desorption.

3.4. DETCHEM^{MONOLITH}

The engine test bench experiments carried out at transient conditions need to include transient heat transfer models. Therefore, these simulations (Section 4.2) were carried out using the code DETCHEM^{MONOLITH}, which couples a transient three-dimensional heat balance of the monolithic structures with simulations of the processes in a number of representative single channels (using DETCHEM^{CHANNEL}). For details we refer to [13,18,48].

[4] Selective catalytic reduction of NO_x with hydrocarbons.

4. Results and discussion

4.1. Simulations of flat bed reactor experiments

For the simulations of the laboratory experimental data, the catalyst specifications from Table 1 and the input data listed in Table 6 were used. Due to the isothermal conditions of the flat bed reactor, the channel wall temperature is assumed to be constant. In order to account for the diffusion of the reactants into the washcoat an effectiveness factor model has been applied with NO as the rate limiting species. Simulations for the Pt/Al_2O_3 model catalyst (10319) have been performed at temperatures of 250, 350, and 450 °C.

NO oxidation: One focus of this work is modeling of NO oxidation in an oxygen-rich atmosphere. At lower temperatures the conversion is limited by kinetics. However, at approximately 320 °C the conversion of NO to NO_2 is restricted by thermodynamic equilibrium and above 420 °C nitrogen oxide becomes the more stable compound. In Fig. 1 a comparison between the simulated NO and NO_2 concentration with the thermodynamic equilibrium concentration is displayed. The inlet concentrations are 250 ppm NO and 12 vol.% O_2 in noble gas. It should be mentioned that the predicted NO_x concentrations at higher temperatures are on the same curve as the thermodynamic equilibrium.

Numerically calculated surface coverage on Pt: In Fig. 2 the numerically calculated surface coverages at the channel exit are displayed for the lean and rich phase. In the oxygen-rich phase the condition of the Pt surface is mainly determined by the ignition of the CO oxidation. Below 180 °C the surface is mainly covered by carbon monoxide. After ignition, CO and oxygen surface species compete strongly and O(s) becomes the most abundant surface species. With higher temperatures the number of free platinum sites increases, so that at 400 °C about 10% of active sites are unoccupied. Upon onset of conversion of nitrogen oxides at 175 °C, surface coverage of NO(s) decreases continuously. On the other hand, the number of adsorbed NO_2(s) increases but is about a magnitude lower than for NO(s). Carbon dioxide adsorption and formation of water on platinum under the conditions investigated are extremely low. Adsorbed water dissociates to O(s) and OH(s) very fast, resulting in high coverage with hydroxyl species.

Under rich exhaust gas conditions the platinum surface is mostly covered with carbon monoxide due to its high sticking coefficient. At 375 °C the surface coverage with CO(s) slightly declines and at 525 °C the majority of active sites is available for adsorption, since the adsorption/desorption equilibrium is shifted to desorption. Coverage with adsorbed oxygen is not depicted here since carbon monoxide is blocking active sites for the dissociative adsorption of O_2. Furthermore, hydrogen also possesses a higher sticking coefficient than oxygen and therefore the platinum surface coverage with H(s) is about 1% at all temperatures.

Table 6
Input data for the simulations.

Surface site density (Γ_{Pt})	2.72×10^{-9} mol/cm^2
Gas velocity	4.56 m/s (25 °C)
Effectiveness factor species	NO

4.1.1. Simulations of experiments under steady-state conditions

In the isothermal experiments under steady-state exhaust gas composition, the influence of carbon monoxide and propylene on NO oxidation in the lean phase and of hydrogen on NO reduction in the rich phase have been investigated. The results are provided as function of catalyst length in order to gain valuable information about inhibition effects and diffusion limitations, which would not have been observable by comparing mole fraction at the channel exit. Moreover, the space velocity (SV) is 40,000 h^{-1} for a catalyst length of 20 cm, but for 16 cm and 8 cm SV increases to values of 50,000 and 100,000 h^{-1}, respectively. Therefore, the validity of simulation results can be compared not only for a single space velocity, but also up to 100,000 h^{-1}, which is a peak value for passenger cars [22].

In both lean and rich phases and at the three temperatures of 250, 350 and 450 °C, the inlet NO concentration is 200 ppm. In the lean phase the CO concentration is varied from 0 to 0.08 vol.% and the C_3H_6 concentration from 0 to 90 ppm (cp. Table 3). The hydrogen mole fraction in the rich exhaust gas composition (Table 4) lies between 0 and 1 vol.%.

4.1.1.1. Lean phase. In Figs. 3 and 4 the influence of CO and C_3H_6 on the oxidation of nitrogen oxide is depicted. According to the diagram at 250 °C the conversion of NO at the entrance of the catalyst is inhibited by both CO and C_3H_6. The simulated NO concentration in the absence of carbon monoxide shows no inhibition and without propylene only minor inhibition at the channel entrance. However, even small amounts of CO or C_3H_6 can inhibit the oxidation of nitrogen oxide by blocking adsorption sites for the dissociative adsorption of oxygen. Surface bound oxygen is

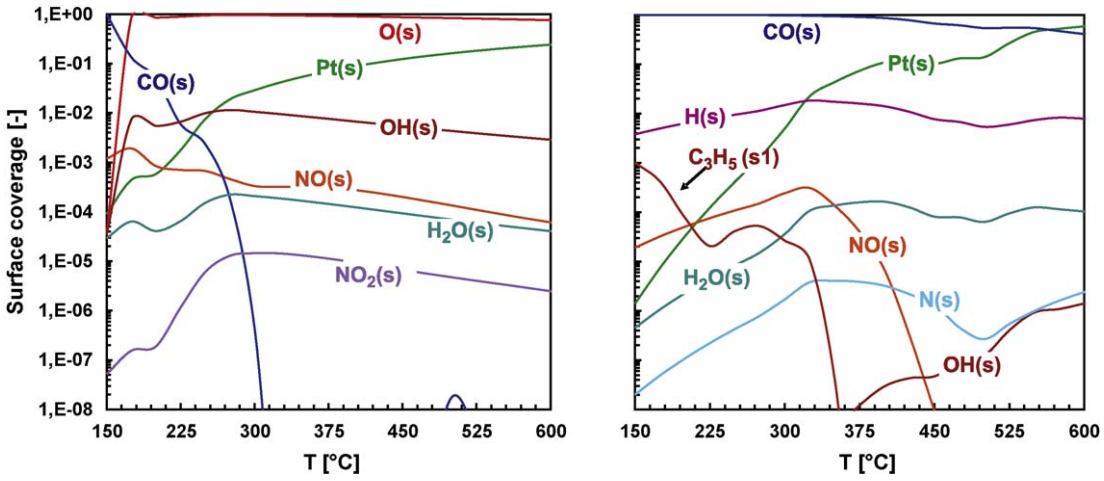

Fig. 2. Simulated surface coverages (logarithmic scale) on platinum at steady-state conditions as a function of temperature, values taken at channel outlet; lean phase (left), rich phase (right), gas composition listed in Table 2.

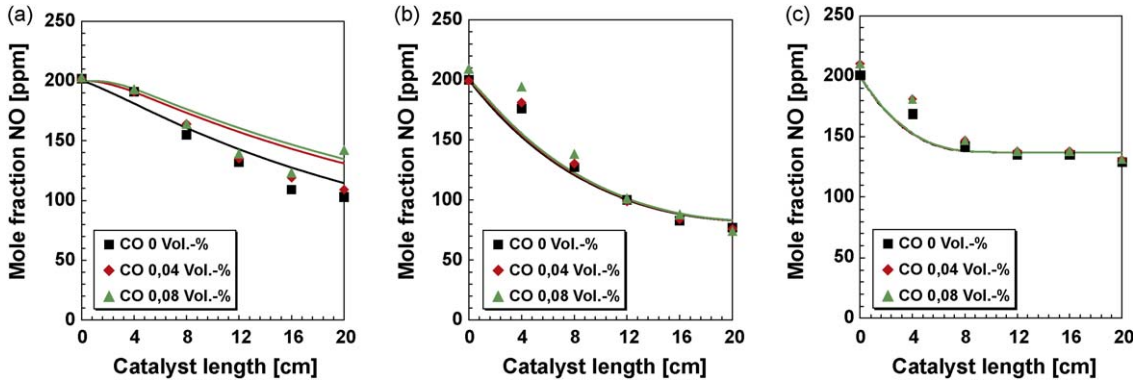

Fig. 3. Influence of CO concentration on the NO oxidation on Pt/Al_2O_3 under steady-state lean conditions at various temperatures; comparison of experiment (□, ◇, △) and simulation (—), gas composition: 200 ppm NO, 60 ppm C_3H_6, 12 vol.% O_2, 7 vol.% CO_2, 10 vol.% H_2O, balance N_2. (a) 250 °C; (b) 350 °C; (c) 450 °C.

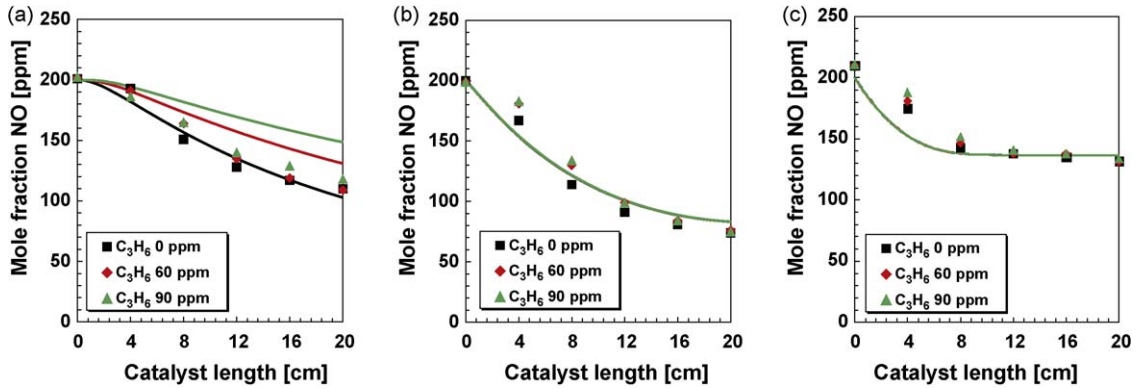

Fig. 4. Influence of C_3H_6 concentration on the NO oxidation on Pt/Al_2O_3 under steady-state lean conditions at various temperatures; comparison of experiment (□, ◇, △) and simulation (—), gas composition: 200 ppm NO, 0.04 vol.% CO, 12 vol.% O_2, 7 vol.% CO_2, 10 vol.% H_2O, balance N_2. (a) 250 °C; (b) 350 °C; (c) 450 °C.

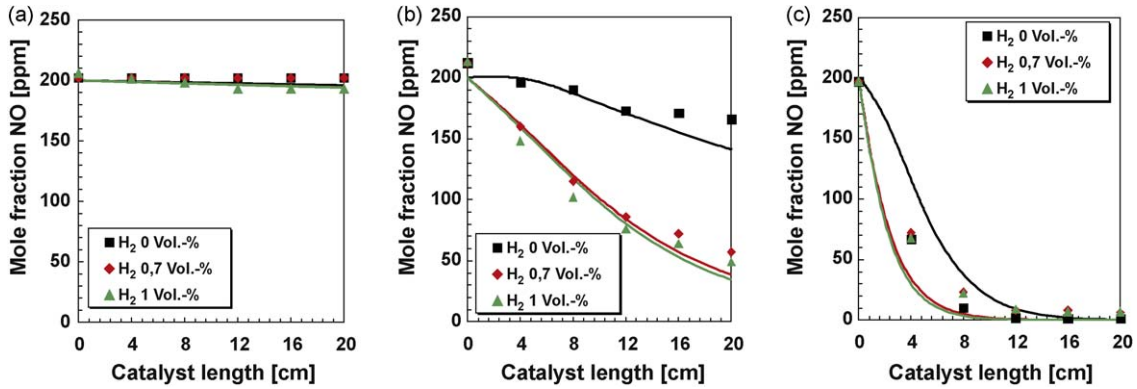

Fig. 5. Influence of H_2 concentration on the NO reduction on $Pt/Pt/Al_2O_3$ under steady-state rich conditions at various temperatures; comparison of experiment (□, ◇, △) and simulation (—), gas composition: 200 ppm NO, 2.1 vol.% CO, 60 ppm C_3H_6, 0.9 vol.% O_2, 7 vol.% CO_2, 10 vol.% H_2O, balance N_2. (a) 250 °C; (b) 350 °C; (c) 450 °C.

crucial for both reaction pathways – Langmuir–Hinshelwood or Eley–Rideal mechanism – for NO oxidation. Interesting to mention is that neither the presence of CO only nor C_3H_6 only is sufficient for a strong inhibiting effect. At higher temperatures no limitation is detectable, because the conversion of nitrogen oxide is constrained by thermodynamics and not by kinetics, cp. Fig. 1.

4.1.1.2. Rich phase. The simulated mole fraction of NO in the rich phase is depicted in Fig. 5. Independently of the presence of hydrogen, the reduction of NO at 250 °C does not take place since the high coverage with CO is blocking the platinum surface as shown in Fig. 2. There are not enough free active sites available for NO dissociation, which is the major step in the CO and C_3H_6 reduction pathway. Moreover, reduction of nitrogen oxide by hydrogen is not feasible due to a low reaction rate. The activation energy of this reaction is increased significantly by high coverages with carbon monoxide, as shown in the detailed reaction mechanism in Table 7. At 350 and 450 °C, even in the absence of hydrogen, NO reduction is pronounced. For the reduction of nitrogen oxide the presence of H_2 is more important than the concentration of the reducing agent, since only slight differences are observable comparing 0.7 and 1 vol.% H_2.

Table 7
Detailed surface reaction mechanism on platinum.

	A (mole, cm, s)	E_a (kJ/mol)
Adsorption/desorption reactions		
$C_3H_6 + Pt(s) + Pt(s) \rightarrow C_3H_6(s)$	$S^0 = 0.98$	
$C_3H_6(s) \rightarrow Pt(s) + Pt(s) + C_3H_6$	3.7×10^{12}	74.4
$C_3H_6 + Pt(s) + O(s) \rightarrow C_3H_5(s) + OH(s)$	$S^0 = 0.05$	
	$\mu(\Theta_{Pt(s)}) = -0.9$	
$C_3H_5(s) + OH(s) \rightarrow O(s) + Pt(s) + C_3H_6$	3.7×10^{21}	31.0
$CH_4 + Pt(s) + Pt(s) \rightarrow CH_3(s) + H(s)$	$S^0 = 0.01$	
$O_2 + Pt(s) + Pt(s) \rightarrow O(s) + O(s)$	$S^0 = 0.07$	
$O(s) + O(s) \rightarrow Pt(s) + Pt(s) + O_2$	3.2×10^{21}	224.7
		$-120\Theta_{O(s)}$
$H_2 + Pt(s) + Pt(s) \rightarrow H(s) + H(s)$	$S^0 = 0.046$	
	$\mu(\Theta_{Pt(s)}) = -1$	
$H(s) + H(s) \rightarrow Pt(s) + Pt(s) + H_2$	2.1×10^{21}	69.1
		$-6\Theta_{H(s)}$
$H_2O + Pt(s) \rightarrow H_2O(s)$	$S^0 = 0.75$	
$H_2O(s) \rightarrow Pt(s) + H_2O$	5.0×10^{13}	49.2
$CO_2 + Pt(s) \rightarrow CO_2(s)$	$S^0 = 0.005$	
$CO_2(s) \rightarrow Pt(s) + CO_2$	3.6×10^{10}	23.7
$CO + Pt(s) \rightarrow CO(s)$	$S^0 = 0.84$	
$CO(s) \rightarrow Pt(s) + CO$	2.1×10^{13}	136.2
		$-33\Theta_{CO(s)}$
$NO + Pt(s) \rightarrow NO(s)$	$S^0 = 0.85$	
$NO(s) \rightarrow Pt(s) + NO$	2.1×10^{12}	80.7
$NO_2 + Pt(s) \rightarrow NO_2(s)$	$S^0 = 0.9$	
$NO_2(s) \rightarrow Pt(s) + NO_2$	1.4×10^{13}	61.0
$N_2O + Pt(s) \rightarrow N_2O(s)$	$S^0 = 0.025$	
$N_2O(s) \rightarrow Pt(s) + N_2O$	1.2×10^{10}	0.7
$N(s) + N(s) \rightarrow Pt(s) + Pt(s) + N_2$	3.7×10^{21}	113.9
		$-75\Theta_{CO(s)}$
Surface reactions		
Propylene oxidation		
$C_3H_6(s) \rightarrow C_3H_5(s) + H(s)$	1.0×10^{13}	75.4
$C_3H_5(s) + H(s) \rightarrow C_3H_6(s)$	3.7×10^{21}	48.8
$C_3H_5(s) + Pt(s) \rightarrow C_2H_3(s) + CH_2(s)$	3.7×10^{21}	108.2
$C_2H_3(s) + CH_2(s) \rightarrow C_3H_5(s) + Pt(s)$	3.7×10^{21}	3.3
$C_2H_3(s) + Pt(s) \rightarrow CH_3(s) + C(s)$	3.7×10^{21}	46.0
$CH_3(s) + C(s) \rightarrow C_2H_3(s) + Pt(s)$	3.7×10^{21}	46.5
$CH_3(s) + Pt(s) \rightarrow CH_2(s) + H(s)$	1.3×10^{22}	70.4
$CH_2(s) + H(s) \rightarrow CH_3(s) + Pt(s)$	2.9×10^{22}	0.4
$CH_2(s) + Pt(s) \rightarrow CH(s) + H(s)$	7.0×10^{22}	59.2
$CH(s) + H(s) \rightarrow CH_2(s) + Pt(s)$	8.1×10^{21}	0.7
$CH(s) + Pt(s) \rightarrow C(s) + H(s)$	3.1×10^{22}	0.0
$C(s) + H(s) \rightarrow CH(s) + Pt(s)$	5.8×10^{21}	128.9
$C_3H_5(s) + O(s) \rightarrow C_3H_4(s) + OH(s)$	5.0×10^{21}	70.0
$C_3H_4(s) + 4\,O(s) + 2\,Pt(s) \rightarrow 3\,C(s) + 4\,OH(s)$	2.6×10^{64}	0.0 [a]
	$\mu(\Theta_{O(s)}) = -3$	$\mu(\Theta_{Pt(s)}) = -1$
$C_2H_3(s) + O(s) \rightarrow CH_3CO(s) + Pt(s)$	3.7×10^{19}	62.3
$CH_3CO(s) + Pt(s) \rightarrow C_2H_3(s) + O(s)$	7.9×10^{20}	191.4
		$+60\Theta_{O(s)}$
$CH_3(s) + CO(s) \rightarrow CH_3CO(s) + Pt(s)$	3.7×10^{21}	82.9
$CH_3CO(s) + Pt(s) \rightarrow CH_3(s) + CO(s)$	1.8×10^{23}	6.1
		$+33\Theta_{CO(s)}$
$CH_3(s) + O(s) \rightarrow OH(s) + CH_2(s)$	3.7×10^{21}	36.6
$OH(s) + CH_2(s) \rightarrow CH_3(s) + O(s)$	2.3×10^{22}	26.0
$CH_2(s) + O(s) \rightarrow OH(s) + CH(s)$	3.7×10^{21}	25.1
$OH(s) + CH(s) \rightarrow CH_2(s) + O(s)$	1.2×10^{21}	26.8
$CH(s) + O(s) \rightarrow OH(s) + C(s)$	3.7×10^{21}	25.1
$OH(s) + C(s) \rightarrow CH(s) + O(s)$	1.9×10^{21}	214.2
Carbon monoxide oxidation		
$CO(s) + O(s) \rightarrow CO_2(s) + Pt(s)$	3.7×10^{20}	108.0
		$+90\Theta_{NO(s)}$
		$-33\Theta_{CO(s)}$
$CO_2(s) + Pt(s) \rightarrow CO(s) + O(s)$	4.0×10^{21}	165.6
		$+60\Theta_{O(s)}$
$C(s) + O(s) \rightarrow CO(s) + Pt(s)$	3.7×10^{21}	0.0
		$+33\Theta_{CO(s)}$
$CO(s) + Pt(s) \rightarrow C(s) + O(s)$	1.7×10^{21}	205.4
		$+60\Theta_{O(s)}$
Reactions of hydroxyl species		
$H(s) + O(s) \rightarrow OH(s) + Pt(s)$	3.7×10^{20}	70.5
$OH(s) + Pt(s) \rightarrow H(s) + O(s)$	1.0×10^{21}	130.7
$OH(s) + H(s) \rightarrow H_2O(s) + Pt(s)$	3.7×10^{21}	17.4
$H_2O(s) + Pt(s) \rightarrow OH(s) + H(s)$	6.8×10^{20}	67.6
$OH(s) + OH(s) \rightarrow H_2O(s) + O(s)$	3.7×10^{21}	48.2
$H_2O(s) + O(s) \rightarrow OH(s) + OH(s)$	2.5×10^{20}	38.2
$CO(s) + OH(s) \rightarrow HCOO(s) + Pt(s)$	3.7×10^{21}	94.2
$HCOO(s) + Pt(s) \rightarrow CO(s) + OH(s)$	1.3×10^{21}	0.9
$HCOO(s) + O(s) \rightarrow OH(s) + CO_2(s)$	3.7×10^{21}	0.0
$OH(s) + CO_2(s) \rightarrow HCOO(s) + O(s)$	2.8×10^{21}	151.1
$HCOO(s) + Pt(s) \rightarrow H(s) + CO_2(s)$	3.7×10^{21}	0.0
$H(s) + CO_2(s) \rightarrow HCOO(s) + Pt(s)$	2.8×10^{21}	90.1
Reactions of NO and NO_2		
$NO(s) + Pt(s) \rightarrow N(s) + O(s)$	5.0×10^{20}	107.8
		$+33\Theta_{CO(s)}$
$N(s) + O(s) \rightarrow NO(s) + Pt(s)$	1.0×10^{21}	122.6
		$-60\Theta_{O(s)}$
$O(s) + NO \rightarrow NO_2(s)$	2.0×10^{13}	111.3
		$+75\Theta_{CO(s)}$
		$-60\Theta_{O(s)}$
$NO_2(s) \rightarrow O(s) + NO$	3.3×10^{14}	115.5
$N(s) + NO(s) \rightarrow N_2O(s) + Pt(s)$	1.0×10^{21}	90.9
$N_2O(s) + Pt(s) \rightarrow N(s) + NO(s)$	2.9×10^{24}	133.1
$O(s) + NO(s) \rightarrow NO_2(s) + Pt(s)$	1.3×10^{17}	133.0
		$+75\Theta_{CO(s)}$
$NO_2(s) + Pt(s) \rightarrow O(s) + NO(s)$	8.1×10^{18}	58.0
$H(s) + NO(s) \rightarrow OH(s) + N(s)$	1.2×10^{21}	25.0
		$+80\Theta_{CO(s)}$
$OH(s) + N(s) \rightarrow H(s) + NO(s)$	6.4×10^{21}	99.9
$NO_2(s) + H(s) \rightarrow OH(s) + NO(s)$	3.9×10^{21}	20.0
$OH(s) + NO(s) \rightarrow NO_2(s) + H(s)$	6.1×10^{22}	175.3

S^0 denotes the initial sticking coefficient. The additional coverage dependency of the kinetic data, Eq. (8), is only stated below relevant reaction equations. This mechanism can be downloaded from www.detchem.com.

[a] Modeled as lumped step.

4.1.2. Simulation of lean/rich cycling experiments

Experimental results for the Pt/Al_2O_3 model catalyst and model-predicted concentrations under cycling lean/rich conditions are pictured in Fig. 6. The composition of the synthetic exhaust gas is listed in Table 2. The experimental concentrations of NO and NO_2 scatter over a range of ±30 ppm. However, no time-dependent variations of the mole fractions could be detected, therefore, steady-state of flow and surface coverage is assumed.

The NO_x feed concentrations in the lean as well as rich phase are 200 ppm NO and 40 ppm NO_2. At 250 and 350 °C NO conversion of about 60% is accomplished, which is shown in Fig. 6. However, maximum conversion is achieved at approximately 280 °C as seen in Fig. 1. At higher temperatures the NO_2 concentration is restricted by the thermodynamic equilibrium, thus only 20% of the NO is converted to NO_2. In the rich phase, at 250 °C, no reduction of nitrogen oxide takes place whereas nitrogen dioxide is already completely reduced due to its higher reactivity. At 350 °C about 75% of the NO_x feed is converted to nitrogen but for complete reduction higher temperatures are necessary. Side reactions to N_2O are implemented in the elementary-step reaction mechanism, but could not be detected experimentally under these reaction conditions. In rich exhaust gas mixtures the coverage with N(s) is too low on the platinum surface for the formation of nitrous oxides. More likely is recombination of adsorbed nitrogen atoms and subsequent desorption.

The flat bed reactor with lateral outlets allows determination of concentration profiles along the catalyst length. The computed and experimentally measured axial profiles of NO, NO_2, and C_3H_6 at the investigated temperatures are depicted in Fig. 7. It is worth to note that, at 250 °C, NO concentration initially increases until the oxidation to NO_2 starts. A comparison of the axial profile of propylene (CO profile is analogous) and NO reveals that nitrogen oxide is converted to NO_2 only after carbon monoxide and propylene are oxidized. By means of the computed surface coverages in the lean phase, it could be shown that it is mainly

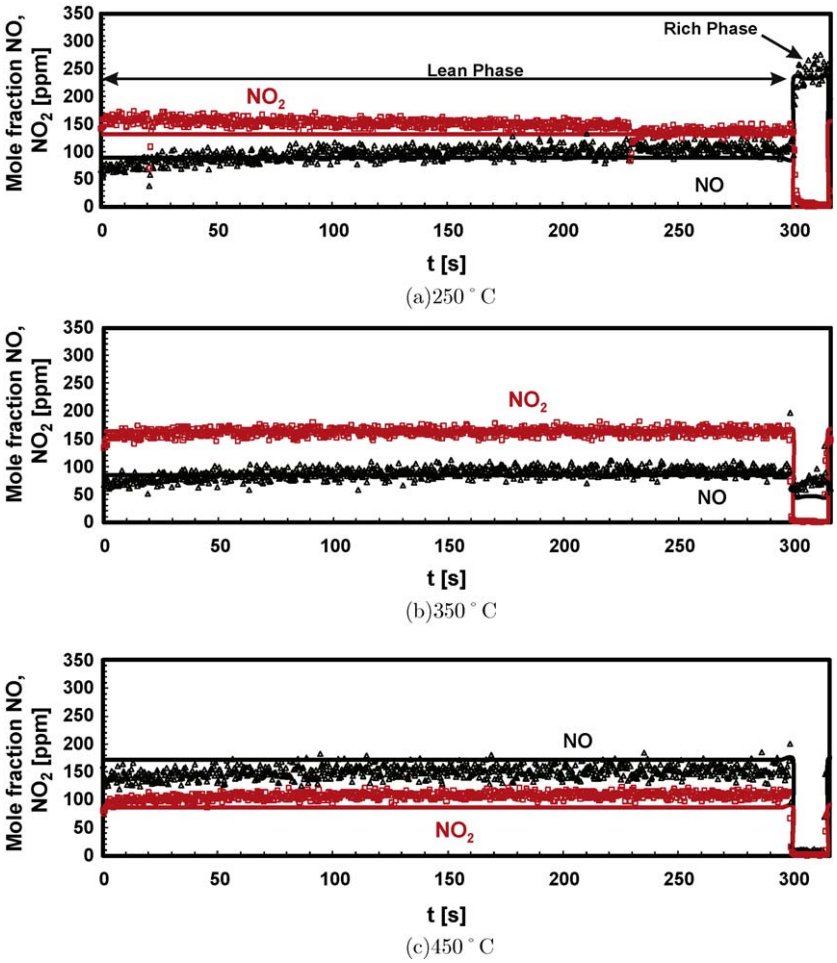

Fig. 6. Lean/rich cycle of 300 s/15 s on Pt/Al_2O_3 at various temperatures; Comparison of experiment (△, □) and simulation (—), gas composition listed in Table 2. (a) 250 °C; (b) 350 °C; (c) 450 °C.

the oxidation of CO that provides free platinum sites for the decomposition of NO_2, leading to increase NO concentration within the first centimeters. At higher temperatures nitrogen oxide is immediately converted to nitrogen dioxide without prior reduction, because oxidation of CO and C_3H_6 is explicitly faster.

4.2. Simulations of engine test bench experiments

The developed quasi-elementary-step reaction mechanism on platinum has been applied for the numerical simulation of transient experiments with a commercial Pt/Al_2O_3 catalyst (HPT) in a dynamic engine test bench. Based upon the steady-state channel simulations with DETCHEM^{CHANNEL} described in Section 4.1, the behavior of the whole monolith under transient conditions has been simulated with DETCHEM^{MONOLITH}[13,48] in order to verify the universal validity of the reaction mechanism. Moreover, one can check the applicability of the platinum mechanism for the prediction of cumulative emissions during a certification cycle.

Under the conditions of the test bench using a gasoline engine and stoichiometric exhaust gas composition ($\lambda \approx 1$), the platinum catalyst functions as a three-way catalyst. This is in contrast to the flat bed reactor experiments, where synthetic lean ($\lambda > 1$) and rich ($\lambda < 1$) diesel exhaust gas mixtures have been used, i.e., we apply now the mechanism at completely different conditions.

For the numerical simulation of the emissions, the composition of the exhaust gas has to be known. Therefore some simplifications had to be taken into account, since not all gas compounds could be measured during the experiments. Generally, neither hydrogen nor water content is determined experimentally. Thus, they had to be calculated from the concentrations of CO and CO_2. It is assumed that CO/H_2 are in equilibrium at a ratio of 3:1 due to the water-gas-shift reaction during the combustion process. The H_2O fraction of the exhaust gas is 0.863 times the CO_2 mass fraction because of the given H/C ratio of the fuel. Furthermore, the content of unburned hydrocarbons is given only in terms of a total hydrocarbon (THC) fraction. A detailed breakdown of the product distribution is not possible, since the exhaust gas contains more than 100 different HC species depending on the engine and its operating point [22–24]. For the simulations, the THC content is grouped into fast-reacting and slow-reacting hydrocarbons. As model hydrocarbons methane for slow-reacting alkanes and propylene as representative for fast-reacting olefins and aromatics are taken into account. In the simulations, the hydrocarbons are partitioned to 95% C_3H_6 and 5% CH_4, which is a realistic product distribution for medium size passenger cars with gasoline engine [24].

Pore diffusion limitation is taken into account by applying an effectiveness-factor washcoat model with CO as rate determining species. The thermo-physical properties of the catalyst (including canning) that were used for the numerical simulations are listed in Table 8.

As aforementioned in Section 2, an uncoated monolith has been installed in front of the platinum catalyst in order to cushion the temperature ramp during the new European driving cycle for a better determination of the light-off, cp. Fig. 8. Furthermore, the

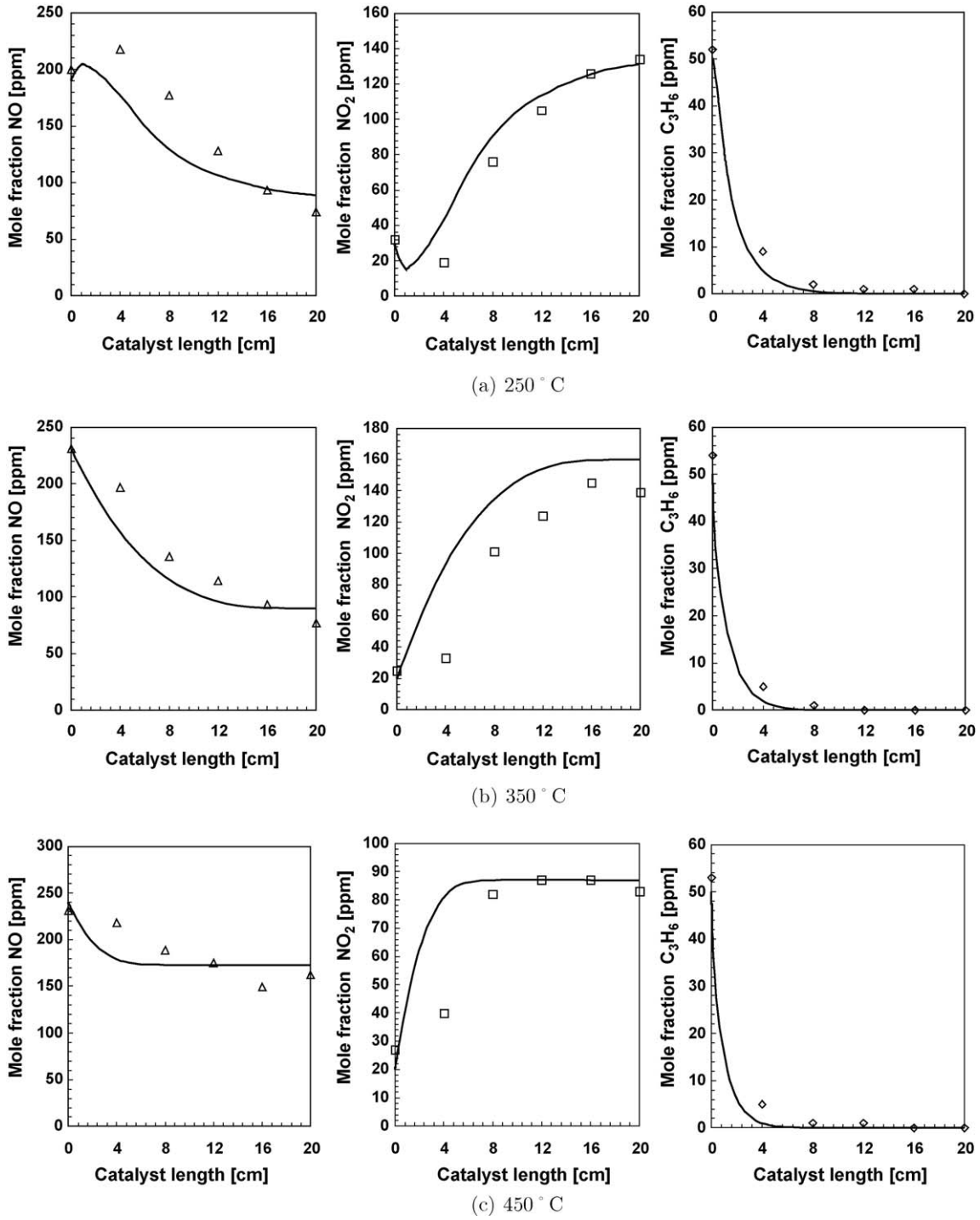

Fig. 7. Axial profiles of NO, NO_2 and C_3H_6 during the lean phase of lean/rich cycling at various temperatures; comparison of experiment (△, □, ◇) and simulation (−). (a) 250 °C; (b) 350 °C; (c) 450 °C.

Table 8
Thermophysical properties of the catalyst, the isolation and the canning.

	Monolith	Isolation	Canning
Heat conductivity (axial) (W/m K)	0.44 [a]	0.1 [a]	25
Heat conductivity (radial) (W/m K)	0.30 [a]	0.1 [a]	25
Heat capacity(J/g K)	0.7 [a]	0.8	0.43
Density (kg/m^3)	540	969	7700

[a] Value at 25 °C. The temperature dependency is described in the simulations by cubic polynomials.

catalyst length is significantly shorter than in real automotive applications. Common catalyst systems usually achieve NO, CO and HC conversion above 95% which result in very low emission of the pollutants. Testing the predictability of the proposed reaction mechanism against experimental reference data with absolute low emission values is not reasonable. Thus, the catalyst length has been modified in order to gain 40–50% conversion for the major pollutants. Experimental data and simulation results for the cumulative emissions of THC, CO, and NO during the NEDC are depicted in Fig. 9.

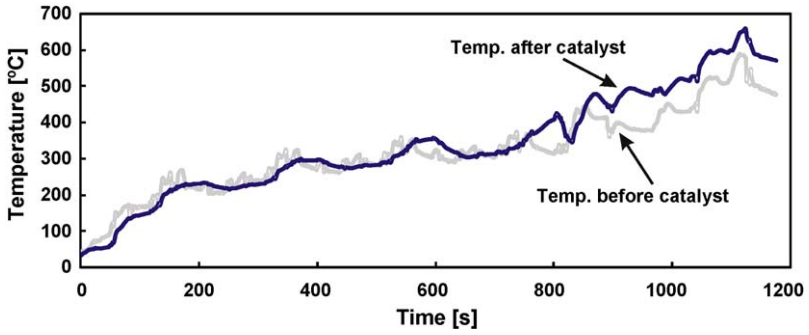

Fig. 8. Measured temperature before (in front of) and after (behind) the Pt/Al_2O_3 catalyst during NEDC as a function of time, cushioned temperature ramp due to additional uncoated monolith prior to the platinum catalyst.

The hydrocarbon emissions during the driving cycle continuously increase until the light-off temperature is reached. The conversion of the hydrocarbons begins after 560 s in the numerical simulations which corresponds to a light-off temperature of about 350 °C in Fig. 8. In the experiments a precise light-off temperature cannot be identified, but the measured temperature in Fig. 8 separates from the temperature of the inlet gas flow after 760 s due to the exothermic oxidation reactions. However, in both simulations and experiments, light-off commences after 820 s indicated by only a slight increase of the cumulative emissions.

The cumulative emissions of CO exhibit a similar behavior like the THC emissions. Carbon monoxide is oxidized at temperatures above 300 °C, which is accomplished after about 560 s in the

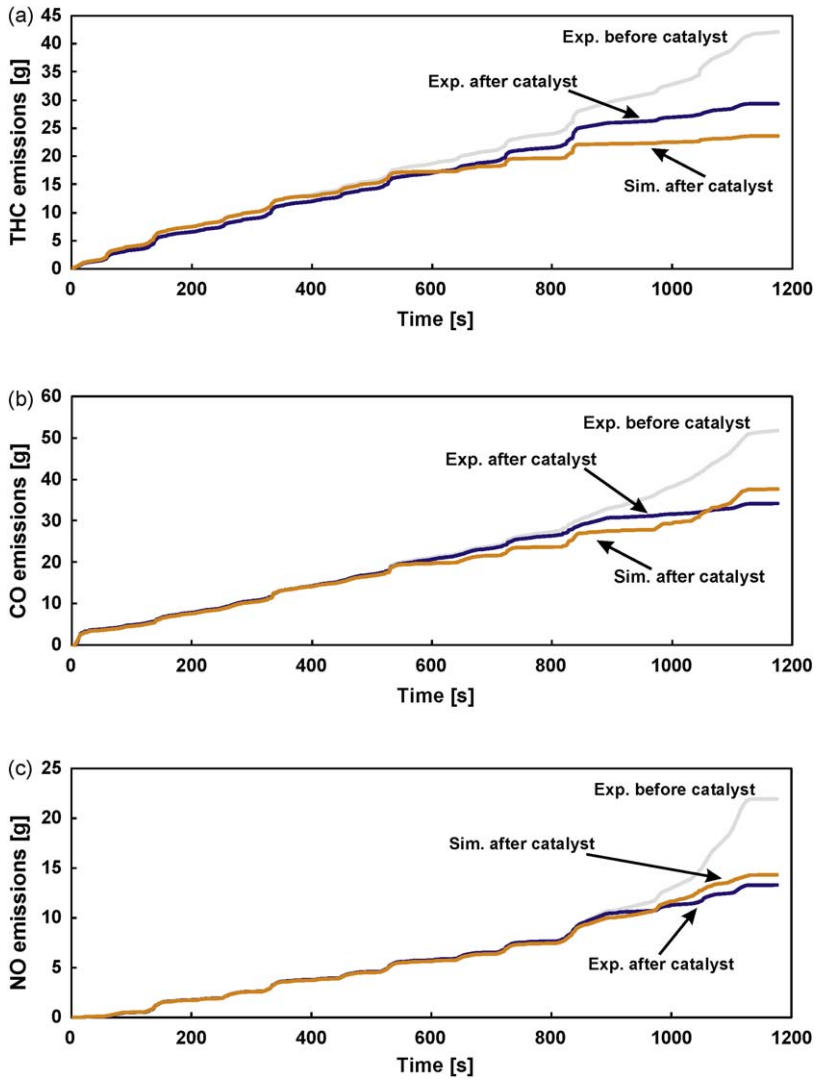

Fig. 9. Cumulative emissions of (a) THC, (b) CO and (c) NO of a commercial Pt/Al_2O_3 catalyst during NEDC as a function of time; comparison of experimental and simulated data.

simulations. In the experimentally measured temperature profile a second peak after 820 s can be detected, which also corresponds to the light-off of the exothermic carbon monoxide oxidation. The conversion of CO increases to about 80% at that point.

The cumulative emissions of NO[5] correspond to the behavior of CO, because under stoichiometric conditions the reduction reaction to nitrogen and carbon dioxide takes place. This reaction is based upon locally free platinum sites provided by the oxidation of carbon monoxide. Before the CO oxidation light-off, the platinum surface is blocked by adsorbed carbon monoxide, which is also displayed in Fig. 2 for a different exhaust gas composition. Only by removing CO from the surface, enough active sites become available for NO dissociation.

Overestimation of the hydrocarbon oxidation resulting in oxygen depletion in the simulations causes the steep increase of the calculated emissions of CO and NO after about 1000 s. Due to the rich atmosphere (lack of oxygen), the platinum surface is poisoned by CO and neither carbon monoxide oxidation nor NO dissociation can take place. The discrepancy between the simulated and experimental values is mainly based upon the simplification of the hydrocarbon mixture represented by methane and propylene. The exact light-off can be adjusted by tuning the CH_4/C_3H_6 ratio, since a larger methane content shifts the temperature to higher values. Nevertheless, we have chosen to keep the literature value which is in compliance with data from the engine manufacturer. Secondly, realistic temperature ramps of 3 K/s during certification cycles reach 500 °C within the first 200 s even after cold starts [49]. Due to the prior installed uncoated monolith, the same temperature is accomplished after 1000 s in our test bench experiments. Hence, deviations in the numerically calculated light-off point of several seconds will diminish during real temperature ramps. Finally, simulations of monolithic reactors with high transient boundary conditions like the NEDC are still very challenging for a detailed modeling approach, because not only kinetics but also thermal behavior of the catalyst has to be modeled properly.

5. Conclusions

A two-dimensional flow-field description with boundary-layer approximation, including a detailed reaction mechanism for the conversion of CO, CH_4, C_3H_6, H_2, O_2 and NO_x has been used to simulate the abatement of automotive exhaust gases on platinum catalysts. The simulations are carried out with the computational tool DETCHEM, which also includes a model for diffusion limitations inside the washcoat.

Based upon experiments with a platinum catalyst in an isothermal flat bed reactor, a detailed surface reaction mechanism has been developed. Numerical simulations of the thermodynamic equilibrium of nitrogen oxides and calculations of surface coverages on platinum have been performed successfully. The simulated concentrations under lean/rich cycling and steady-state lean and rich exhaust gas have been compared to experimental data of the monolithic catalyst. At otherwise constant exhaust gas composition, CO, C_3H_6, and H_2 were varied (component by component) in order to investigate the influence of the components on the conversion of nitrogen oxide. A very good agreement with the numerically calculated data could be achieved in the temperature range of 250 to 450 °C. Furthermore, the simulations predicted the concentration profiles of nitrogen oxides and propylene along the catalyst length under cycling conditions.

As further application of the detailed surface reaction mechanism, experiments with a commercial platinum catalyst in a dynamic engine test bench have been performed. The simulated cumulative emissions of hydrocarbons, CO and NO during a certification cycle matched the experimental data. However, deviation of light-off temperatures was detected. Due to the simplified hydrocarbon mixture consisting of methane and propylene and a cushioned temperature ramp in the experiments, the predicted light-off of THC and CO commences too early. On the other hand, the calculated emission of NO accomplished a high accuracy. Taking into account the complexity of the test bench with its uncertainties describing initial gas composition and boundary conditions, the detailed model performs impressively well for the prediction of cumulative emissions in a test driving cycle. This application clearly shows the benefit of models, which are based on the molecular behavior. Those elementary-steps like reaction mechanisms can also be applied in application at conditions, which had not been tested during model development. It should be highlighted that the original model is used for the test bench simulation as it is, i.e., without fitting of any rate coefficients.

Numerical modeling of monolithic catalytic converters is a very effective tool to investigate the catalyst performance. As a first step, reliable surface mechanisms based upon elementary-step like reactions have to be developed. In this work, we presented a comprehensive surface reaction mechanism on platinum for the conversion of hydrocarbons, CO and NO_x. This mechanism has been validated by comparison with experimental data under lean, rich and stoichiometric exhaust gas composition and, moreover, under isothermal and highly transient conditions. Finally, the mechanism will allow simulations to predict emissions over a broad range of conditions, even though further improvements are still needed.

[5] Engine raw emissions consist usually of 98% NO.

Acknowledgments

The authors would like to gratefully acknowledge the Forschungsvereinigung Verbrennungskraftmaschinen e.V. (FVV) for the financial support and Umicore (formerly Delphi Catalyst) for providing the model catalysts. The authors would also like to thank Volker Schmeisser and Gerhart Eigenberger (University of Stuttgart) for sharing their experimental results which are crucial for the success of this work. Finally, we gratefully acknowledge J. Eberspächer GmbH & Co. KG and Daimler AG for providing the engine test bench results.

References

[1] H. Renner, et al. in: M. Bohnet, F. Ullmann (Eds.), Ullmann's Encyclopedia of Industrial Chemistry, 7th edition, Wiley–VCH, 2007.
[2] R. Heck, R. Farrauto, S. Gulati, Catalytic Air Pollution Control, 2nd edition, Wiley, 2002.
[3] G. Pontikakis, G. Konstantas, A. Stamatelos, Journal of Engineering for Gas Turbines and Power-Transactions of the ASME 126 (4) (2004) 906–923.
[4] P. Koci, M. Kubicek, M. Marek, Industrial & Engineering Chemistry Research 43 (16) (2004) 4503–4510.
[5] C. Depcik, D. Assanis, Progress in Energy and Combustion Science 31 (4) (2005) 308–369.
[6] R. Holder, M. Bollig, D.R. Anderson, J.K. Hochmuth, Chemical Engineering Science 61 (24) (2006) 8010–8027.
[7] D. Chatterjee, T. Burkhardt, M. Weibel, E. Tronconi, I. Nova, Numerical simulation of $NO/NO_2/NH_3$ reactions on SCR-catalytic converters: model development and applications, SAE Technical Paper Series 2006-01-0468.
[8] M. Frey, G. Wenninger, B. Krutzsch, G. Koltsakis, O. Haralampous, Z. Samaras, Topics in Catalysis 42–43 (1–4) (2007) 237–245.
[9] O. Deutschmann, in: G. Ertl, H. Knözinger, F. Schüth, J. Weitkamp (Eds.), Handbook of Heterogeneous Catalysis, 2nd edition, Wiley–VCH, 2008.
[10] M. Rinnemo, O. Deutschmann, F. Behrendt, B. Kasemo, Combustion and Flame 111 (1997) 312–326.
[11] S. Raimondeau, D. Vlachos, Chemical Engineering Science 58 (3–6) (2003) 657–663.
[12] V. Janardhanan, O. Deutschmann, Journal of Power Sources 162 (2) (2006) 1192–1202.

[13] O. Deutschmann, S. Tischer, S. Kleditzsch, V. Janardhanan, C. Correa, D. Chatterjee, N. Mladenov, H. Minh, DETCHEM Software Package, 2.1 edition, www.detchem.-com, Karlsruhe, 2007.
[14] J. Anderson, M. Fernandez Garcia, Supported Metals in Catalysis, Imperial College Press, London, 2005.
[15] V. Schmeisser, J.D. Perez, U Tuttlies, G Eigenberger, Topics in Catalysis 42–43 (1–4) (2007) 15–19.
[16] Robert Bosch GmbH (Ed.), Automotive Handbook, 7th edition, Wiley, Weinheim, 2007.
[17] L. Raja, R. Kee, O. Deutschmann, J. Warnatz, L.D. Schmidt, Catalysis Today 59 (2000) 47.
[18] S. Tischer, C. Correa, O. Deutschmann, Catalysis Today 69 (1–4) (2001) 57–62.
[19] R. Kee, M. Coltrin, P. Glarborg, Chemically Reacting Flow, 1st edition, Wiley–Interscience, 2003.
[20] R. Hayes, S. Kolaczkowski, Introduction to Catalytic Combustion, Gordon and Breach Science Publishers, Amsterdam, 1997.
[21] D. Chatterjee, O. Deutschmann, J. Warnatz, Faraday Discussions 119 (2001) 371–384.
[22] E. Lox, B. Engler, in: G. Ertl, H. Knoezinger, J. Weitkamp (Eds.), Handbook of Heterogeneous Catalysis, VCH, 1997.
[23] T. Kanazawa, K. Sakurai, Development of the automotive exhaust hydrocarbon adsorbent, SAE Technical Paper Series 2001-01-0660.
[24] M. Tanaka, Y. Tsujimoto, T. Miyazaki, M. Warashina, S. Wakamatsu, Chemosphere-Global Change Science 3 (2) (2001) 185–197.
[25] G. Schoofs, C. Arumainayagam, M. McMaster, R. Madix, Surface Science 215 (1–2) (1989) 1–28.
[26] O. Deutschmann, F. Behrendt, J. Warnatz, Catalysis Today 21 (2–3) (1994) 461–470.
[27] D. Hickman, L. Schmidt, AIChE Journal 39 (7) (1993) 1164–1177.
[28] G. Ertl, Surface Science 300 (1–3) (1994) 742–754.
[29] C. Campbell, G. Ertl, H. Kuipers, J. Segner, Surface Science 107 (1) (1981) 207–219.
[30] S. Salomons, M. Votsmeier, R. Hayes, A. Drochner, H. Vogel, J. Gieshof, Catalysis Today 117 (4) (2006) 491–497.
[31] J. Barbier, D. Duprez, Applied Catalysis B: Environmental 4 (2–3) (1994) 105–140.
[32] A. Zeigarnik, C. Callaghan, R. Datta, I. Fishtik, E. Shustorovich, Kinetics and Catalysis 46 (4) (2005) 509–515.
[33] M. Crocoll, S. Kureti, W. Weisweiler, Journal of Catalysis 229 (2) (2005) 480–489.
[34] R. Burch, T. Watling, Journal of Catalysis 169 (1) (1997) 45–54.
[35] L. Olsson, B. Westerberg, H. Persson, E. Fridell, M. Skoglundh, B. Andersson, Journal of Physical Chemistry B 103 (47) (1999) 10433–10439.
[36] L. Olsson, H. Persson, E. Fridell, M. Skoglundh, B. Andersson, Journal of Physical Chemistry B 105 (29) (2001) 6895–6906.
[37] S. Mulla, N. Chen, W. Delgass, W. Epling, F. Ribeiro, Catalysis Letters 100 (3–4) (2005) 267–270.
[38] S. Mulla, N. Chen, L. Cumaranatunge, G. Blau, D. Zemlyanov, W. Delgass, W. Epling, F. Ribeiro, Journal of Catalysis 241 (2) (2006) 389–399.
[39] F. Gobal, S. Azizian, Langmuir 13 (22) (1997) 5999–6000.
[40] D. Mei, Q. Ge, M. Neurock, L. Kieken, J. Lerou, Molecular Physics 102 (4) (2004) 361–369.
[41] S. Ovesson, B. Lundqvist, W. Schneider, A. Bogicevic, Physical Review B: Condensed Matter and Materials Physics 71 (11) (2005) 1–5.
[42] R. Getman, W. Schneider, Journal of Physical Chemistry C 111 (1) (2007) 389–397.
[43] D. Parker, B. Koel, Journal of Vacuum Science & Technology A 8 (3) (1990) 2585–2590.
[44] D. Chambers, N. Cant, Applied Catalysis B: Environmental 41 (1–2) (2003) 61–70.
[45] E. Shustorovich, A. Bell, Surface Science 289 (1–2) (1993) 127–138.
[46] N. Macleod, R. Lambert, Applied Catalysis B: Environmental 35 (4) (2002) 269–279.
[47] D. Mantri, P. Aghalayam, Catalysis Today 119 (1–4) (2007) 88–93.
[48] S. Tischer, O. Deutschmann, Catalysis Today 105 (3–4) (2005) 407–413.
[49] R. van Basshuysen, F. Schäfer (Eds.), Internal Combustion Engine Handbook, SAE International, 2004.